E. BALAJI©[1], R. SATHIYA MOORTHY©[2*]

EFFECT OF FRICTION STIR PROCESSING ON THE MICROSTRUCTURE, MECHANICAL AND TRIBOLOGICAL PROPERTIES OF SILICON NITRIDE REINFORCED ZE43 MAGNESIUM COMPOSITE

Magnesium matrix composites are being used in more and more different ways, so they need to have good surface properties like resistance to wear and corrosion. In this work, we used friction stir processing to make ZE43 magnesium surface composites with different amounts of Si_3N_4 particles (by volumes 6.0%, 12.0%, and 18.0%, respectively). X-ray diffraction and scanning electron microscope analysis showed Si_3N_4 particles in the developed magnesium surface composite are all uniformly distributed. After FSP, the composites were tested for hardness. Using Potentio dynamic polarization, the corrosion behavior of both the base matrix material and composites made were studied. The composite containing 18% Si_3N_4 has the highest corrosion resistance .The composite's sliding wear behavior and coefficient of friction analyzed by a pin-on-disc tribometer by changing the amount of Si_3N_4 in the material, load and sliding distance. To attain the highest possible wear resistance and coefficient of friction, parameters of the process were optimized with the help of taguchi grey relational analysis. The results show that load, followed by volumetric percentage, and sliding distance have a substantial effect on wear rate and friction coefficient.

Keywords: FSP; ZE43; Magnesium; Si_3N_4; MMC

1. Introduction

In today's world as technology advances, the demand for high-performance materials with versatile qualities increases across all industries. Traditional materials and their alloys, which are commonly employed in engineering, are no longer able to match the demands of modern applications because of their poor corrosion and wear resistance. One way to overcome these property deficiencies is to add hard reinforcements, mainly ceramic particles to existing engineering materials. These newly created materials are known as metal matrix composites (MMC) [1]. MMCs that are strengthened with ceramic particles can be used in a lot of different places, like automotive parts, in the aerospace industry, in electronic parts, and so on [2]. During their service life, crucial components of the aforementioned applications are exposed to adverse environments. Therefore, its inner and outer materials are subject to scratches, indentations, and wear during operations. Hence, a detailed investigation of the surface behavior of metal matrix composites (MMCs) is necessary [3].Using standard liquid state surface treatment procedures, such as laser melting [4], plasma sprays [5], and e-beam radiation [6], it's not

been possible to disperse reinforcements with little porosity. Also, it has been found that matrix-reinforcement material reactions cause unwanted phases to form when these techniques are used. Further, it is challenging to distribute uniformly the reinforcing particles throughout the magnesium's surface. Therefore, to ensure the reinforcing ceramic particles distributed equally across the surface of base matrix, the surface composite must be produced at temperatures significantly lower than the melting point of base matrix material. Friction stir welding is the base of the Friction Stir Processing technique, which has been investigated by a number of scientists in recent years as a means of producing advanced surface composites with improved surface characteristics, including high hardness, corrosion resistance, wear resistance, etc., [7]. Friction Stir Processing, a surface treatment that happens in the solid state, is one of the most efficient and advanced techniques for improving the surface characteristics of metal matrix composites [8]. It is carried out much below the underlying material's melting point. During the FSP process, metals are exposed to high temperatures when they come into contact with tools made of metal. The material undergoes significant plastic deformation and mixing, which causes a large change in the microstructure.

[1] FACULTY OF ENGINEERING AND TECHNOLOGY,DEPARTMENT OF MECHANICAL ENGINEERING, SRM INSTITUTE OF SCIENCE AND TECHNOLOGY, RAMAPURAM CAMPUS, CHENNAI – 600 089, TAMIL NADU, INDIA

[2] ANNA UNIVERSITY REGIONAL CAMPUS, DEPARTMENT OF MECHANICAL ENGINEERING, COIMBATORE, TAMILNADU, INDIA

* Corresponding author: rsathiyamoorthy@ymail.com

Hence, MMC is formed in the stirred region. Also, the chemical process happens through FSP can result in the creation of in-situ composites [9]. When some ceramic particles are mixed with a matrix material, the surface may get much harder, making it less likely to wear away. Adding ceramic particles to a metal may cause it to become more brittle and mixing materials causes significant microstructural change. Thus, surface composites are receiving more attention [10]. There has been a lot of work done in the composite areas due to the high demands on materials to improve overall performance. It has become more and more important to make materials that are both light and strong.

Researchers have widely used friction stir processing to produce aluminium [11], steel [12], and titanium [13] surface composites. Friction stir processing, as found by Hariom Tripathi et al. refined the micro structure of AZ91 alloy, causing a shift in material's mechanical properties.In addition, the impacts of altering the tool's rotational speed were evaluated [14]. Several authors, including Ahmed Z. Naser, have created surface composites with FSP by mixing SiC powder particles with Mg base metal. The average microhardness was significantly increased using this method [15]. Fei Long et al. used FSP to strengthen Mg-5Zn alloy and make it more resistant to corrosion. Their results showed that by using FSP, the average particle size of Mg-5Zn alloy could be reduced. The corrosion current density flowing through FSPed sample in an aqueous solution containing 3.5 wt.% NaCl was 4.1×10^{-6} A/cm^2, which was much lower than that of the base material [16]. S. Sudhagar et al. made a copper surface composite that was strengthened with Si$_3$N$_4$. They discovered that friction-stir processed surface composites were weaker than untreated copper. As the reinforcement volume percentage goes up, the mechanical characteristics of the developed surface composites gets better [17]. Pabitra Maji et al. incorporated CeO$_2$ and MoS$_2$ particles into the Al7075 alloy using friction stir processing. Tensile strength and microhardness improved by slowing down the processing speed and making more passes. All of the processed composites showed both abrasive and adhesive wear. Microhardness, particulate distribution, and wear resistance were improved in composite produced with a two pass and 30 mm/min feed rate. The composite that was made in a single pass at 30 mm per minute showed the best corrosion resistance [18]. Hardness and microstructures of the AZ31/Al$_2$O$_3$ composite were studied by M. Azizieh et al. by varying the rotational tool speed, the tool pin shape, and the particle size of the ceramics. With each pass of the FSP and faster rotational speeds, the particles were spread out more evenly. Because materials couldn't move as freely in the stir zone, samples were found to have micro-holes and cavities [19]. In other research, particles like ZrO$_2$ [20], CNT [21], SiC [22], and B$_4$C [23] were used with the FSP method to make magnesium alloys stronger. Parthiban Krishnan et al. looked into the fatigue properties and corrosion characteristics of hybrid magnesium nanocomposites. The resistance to corrosion of hybrid nanocomposites was far better than that of base metal. The Mg-Zn alloy's fatigue strength, which has been enhanced by adding 1.5% hBN$_P$ and 1% SiC$_P$, is around 94 MPa, a 41 percent improvement over that of the basic alloy [24]. Titus Thankachan et al. show the use of machine learning models and statistical techniques for forecasting and evaluation of copper-based surface composite wear rates under dry sliding conditions. Through friction stir processing, different percentages of boron nitride particles were put on the surface of copper. Experiments and statistical analysis have shown that BN particles can greatly slow down the rate of wear [25]. This work is about making a surface composite made of magnesium and reinforced with silicon nitride (Si$_3$N$_4$) in different volume percentages. Various researchers have made Mg surface composites with a variety of reinforcements. ZE43 magnesium-surface metal matrix composites have not been studied extensively. In aerospace, magnesium alloy with zinc and rare earth (ZE43) is used [26]. The utilization of nitride reinforcements in the development of magnesium-based composites with rare earth elements is limited. Silicon nitride ceramic reinforcement is an ideal material for producing magnesium metal matrix composites because of its high specific modulus, stability at high temperatures, and low density. It is hard to visually and manually evaluate the process variables that affect the rate of wear and COF of composite materials. For the development of application-specific composites, it is important to find a link between the wear rate of developed composites and their process parameters. Here we use Taguchi based grey relational analysis, which is a simple, inexpensive statistical method backed by ANOVA. In addition to the interaction between each parameter, the volumetric percentage of Si$_3$N$_4$ particles and how they affect the wear properties and COF also need to be evaluated. The primary objective of this research is to focus on the effect of Si$_3$N$_4$ particles on the wear rate and corrosion resistance of Mg-Zn-RE (ZE43)-based surface composites, as well as the effects on surface properties under various testing conditions as the volume percent of Si$_3$N$_4$ increases inside the magnesium metal matrix.

2. Materials and methods

2.1. Materials

In this investigation, plates made of the magnesium alloy ZE43 (Mg-4.1Zn-2.8RE-0.5Zr) measuring length: 150 mm, width: 50 mm, depth: 8 mm were procured to be used as base matrix metal (BM). Silicon nitride (Si$_3$N$_4$) particles with a size between 30 and 40 µm are utilized as reinforcement to change the surface because they have a low density, don't wear down easily, and are stable at high temperatures. In this work, we used Yitrium as the rare earth element.

2.2. Methods

Friction stir processing involves carving a groove in middle of the specimen. The volumetric fraction of reinforcing particles to be packed determines the groove size. A certain amount of Si$_3$N$_4$ particles must be distributed all through the plate, and

this percentage is determined by the width of the groove. Three identical plates were carved to 0.36 mm, 0.72 mm, and 1.08 mm of groove widths and a 4 mm depth to generate three different amounts of Si_3N_4 particles (by volumes of 6.0%, 12.0%, and 18.0% respectively). For this work, we opted for a tool made of H13 steel that had been heat treated twice after rigorous testing and investigation of a variety of tool materials. A cylinder-shaped tool would be perfect for this work because it would help spread the reinforcement material evenly across the surface, making it harder and more resistant to wear. In this case, we employ both pinned and pinless tools. To ensure that the Si_3N_4 particles remained there during friction stir processing, they were initially processed using a pinless tool on the groove's top. The pinched tool's shoulder has a diameter of 16 millimeters. The pin on the shoulder was 5 mm long and 6 mm in diameter. Using a milling machine with a feature for controlling displacement, FSP was performed at a rotational speed of 1200 rpm and a traverse feed of 20 mm/min. By passing the pinned tool over the compacted carved surface one time, the material is deformed for the distribution of reinforcement. Fig. 1 portrays the processes involved in friction stir processing.

Microstructural analysis using an optical microscope was utilized to analyze the generated magnesium surface composites for the impact of friction stir processing and reinforcing particles. Specimens were cut with a wire-cut EDM, cleaned, and etched to metallurgical specifications before being examined under optical microscope. SEM was utilized to examine bonding of reinforcements with the base matrix and dispersion of Si_3N_4 particles within magnesium matrix. Microhardness tests were performed on the composite surfaces that run perpendicular to the directions of processing, as specified by ASTM E384, to assess the hardness variation between the zones. Microhardness of the surface composites that were made was looked into because a material's wear resistance is directly related to its hardness. Three tests were done to make sure that the values for hardness were the same each time.

Corrosion characteristics of the base matrix material and FSPed specimens were determined using Potentio Dynamic Polarization (PDP). In an electrolytic cell with a three-electrode cell arrangement, the polarization curves of the samples were measured. The three-electrode cell consists of a counter electrode (a piece of platinum foil 10 mm × 20 mm), a reference electrode (saturated calomel), and a working electrode (the specimen). The electrolyte in the electrolytic cell is a 3.5 wt.% NaCl solution, and the exposed specimen surface is just 1 cm^2. From a starting point around 2000 millivolts (mV) below the corrosion potential, the polarization increased to a maximum of 50 millivolts (mV) above the corrosion potential. 10 mV/min was maintained as the scanning rate. Corrosion characteristics can be explained with the help of this experiment, which exhibits the relationship involving current and potential. The pin-on-disc wear test equipment was used to conduct the dry sliding wear tests at room temperature as per the ASTM G99 standard. From the center of the stir zone, wear pins measuring 6 mm in diameter were formed and then polished using emery paper of a standard grade. To achieve a good finish on the testing surface, cloth polishing was performed. The E31 hardened steel disc was used as the counter surface. The specimens were weighed.

One of the most effective multi-response optimization methods, Taguchi-based grey relational analysis may be used to solve a variety of design problems [27]. Complex procedures have some good things about them, like being easy to put together quickly and saving money while getting the most use out of them. In this research, the Taguchi method was used in planning orthogonal array experiments. Here the experimental design were carried out using Minitab 19. The most significant steps in experiment design are picking the most influential control factors and choosing a suitable orthogonal array depending on number of levels. For each developed surface composite, a series of tests were done with different Si_3N_4 volume percentages of 6, 12, and 18% under loads of 5, 10 and 15 N and sliding distances of 500, 1000, and 1500 m, respectively. The wear rate can be calculated by comparing the sample's initial and final weights. Also, the coefficient of friction for the corresponding wear rate is also determined. As mentioned above, TABLE 1 shows the selection of three input process parameters across three levels
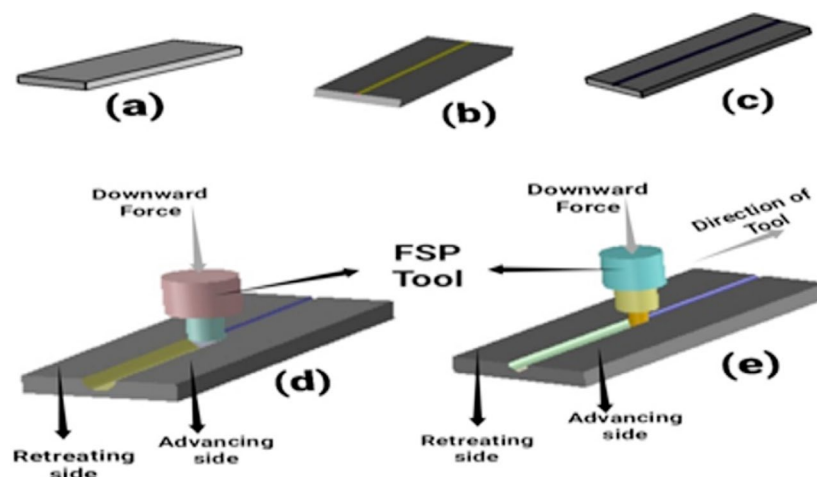
Fig. 1. Friction stir processing (a) Magnesium ZE43 alloy (b) Specimen with a groove in the center (c) Particles of Si_3N_4 compacted in the groove (d) Preprocessing using a pinless tool (e) Employing a pinned tool for processing

for the wear rate and friction coefficient assessment. TABLE 2 displays the L_{27} orthogonal array used in this work to determine the influence of every factor over the wear rate and coefficient of friction of generated composites.

Process parameters as control factors and levels

Control factors	Code	Unit	Level 1	Level 2	Level 3
Volume Percentage	A	%	6	12	18
Load	B	N	5	10	15
Sliding distance	C	m	500	1000	1500

Taguchi's analysis makes use of a well-known statistically reliable analysis known as the signal-to-noise ratio (S/N ratio). Ju-Long developed GRA in 1982 [28]. GRA functions like a discovery concept, bringing together familiar and unfamiliar parts to achieve optimal response. The grey relational co-efficient (GRC) and grey relational grade (GRG) are calculated by GRA by normalizing the values. Forecasting the optimum level of grey relationship grades is made possible through a connection to ANOVA and the computation of the optimal process level. Wear rate and coefficient of friction are important quality factors of friction stir-processed composites. When comparing experimental findings, a greater grey relational grade implies that they are more in line with the normalized value or optimum value. The impact of each factor on the system, however, varies in practice. To illustrate the relationship between sequences, the GRA is applied. When the both sequences are same, GRG equals 1. In addition, GRG also demonstrates the extent to which the contrasting sequence can influence the standard sequence.

3. Results and discussion

The grooves generated on the plate's surface were not visible after friction stir processing on the ZE43 magnesium composites. The ZE43 magnesium underneath the tool portion is plasticized and deformed by the frictional heat produced; moreover, the compressed Si_3N_4 particles were dispersed throughout the plasticized base matrix by the tool's rotating action. Material flow leads to the formation of a stir zone that comprises ZE43/Si_3N_4 composites [29]. Stir region serves as composite zone, and its surface is uniform and free of pinholes.

3.1. Microstructural characterization

It is important to take into account the ceramic particles' grain size and deformation when spreading reinforcements into the composite's surface. Fig. 2 reveals the microstructure of ZE43 magnesium composite FSPed ZE43 magnesium composite, with 6, 12, and 18% silicon nitride by volume. During friction stir processing, intense frictional heat and stirring motion cause grains to break down, causing extreme plastic deformation. The composite is formed by combining the silicon nitride particles, which have been previously positioned in the groove, with the molten magnesium. Due to this plastic deformation, the area where the friction stir processing (FSP) takes place transforms into a metal matrix composite (stir zone). A stir zone is created as a result of the fusion of materials, and it is encompassed by a Heat Affected Zone (HAZ).

The figures clearly show that the FSP was responsible for the ZE43 magnesium matrix's plastic deformation, which led to grain breakage and subsequent grain refining. It is clear that plastic deformation has taken place when comparing Fig. 2(a) and Fig. 2(b-d). As the volume percentage of silicon nitride increases, the spacing between reinforcing particles decreases. Reinforcement particles are spread out evenly because there is effective stirring, frictional heat generation, and the movement of particles in plastic deformation across the stir zone [30]. The generated magnesium ZE43/Si_3N_4 surface composites were characterized by SEM, shown in Fig. 3.

From the figures, it can be seen that the reinforcement particles and matrix are tightly bound due to which the porosity

Taguchi L_{27} OA Experiment design

Trial	Si$_3$N$_4$ vol. (%)	Load (N)	Sliding distance (m)	Trial	Si$_3$N$_4$ vol. (%)	Load (N)	Sliding distance (m)
1	6	5	500	15	18	10	1000
2	12	5	500	16	6	10	1500
3	18	5	500	17	12	10	1500
4	6	5	1000	18	18	10	1500
5	12	5	1000	19	6	15	500
6	18	5	1000	20	12	15	500
7	6	5	1500	21	18	15	500
8	12	5	1500	22	6	15	1000
9	18	5	1500	23	12	15	1000
10	6	10	500	24	18	15	1000
11	12	10	500	25	6	15	1500
12	18	10	500	26	12	15	1500
13	6	10	1000	27	18	15	1500
14	12	10	1000				
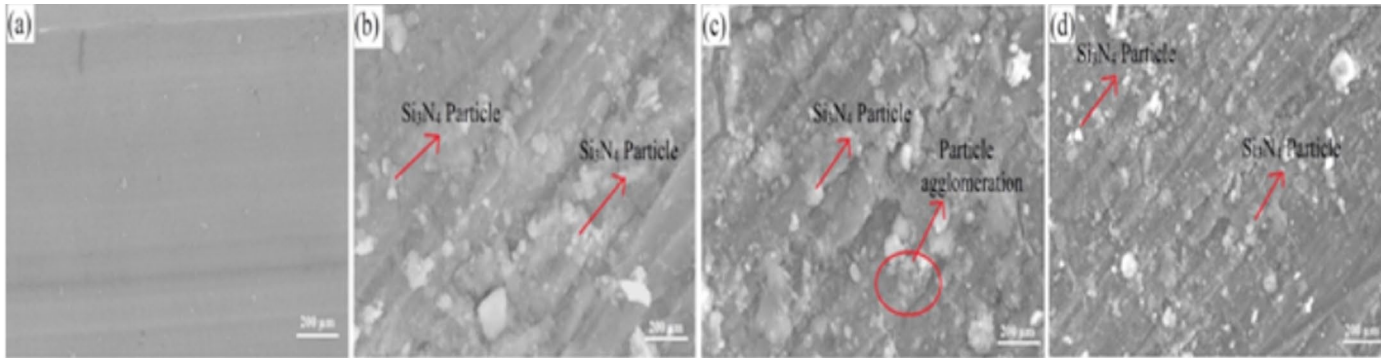
Fig. 2. Visualizations from an optical microscope of (a) Magnesium ZE43 alloy (b) Magnesium ZE43 containing 6% Si$_3$N$_4$ (c) Magnesium ZE43 containing 12% Si$_3$N$_4$ (d) Magnesium ZE43 containing 18% Si$_3$N$_4$
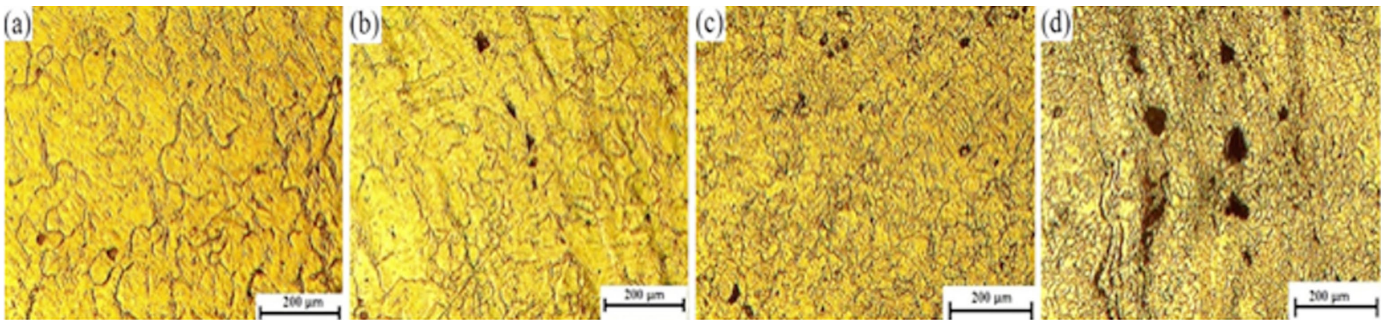
Fig. 3. SEM images of (a) Magnesium ZE43 alloy (b) Magnesium ZE43 containing 6% Si$_3$N$_4$ (c) Magnesium ZE43 containing 12% Si$_3$N$_4$ (d) Magnesium ZSE43 containing 18% Si$_3$N$_4$

has been greatly diminished. The frictional heat is generated due to the rotation of the tool and so there is a rise in temperature in the stir zone. In the FS-processed region, there was no evidence of any micro voids. As shown in Fig. 3(d), Si$_3$N$_4$ was found to be uniformly distributed throughout the FSP region.

The SEM results show that grain growth decreases noticeably as the volume percentage of Si$_3$N$_4$ goes up. This may be because of the "pinning effect." Furthermore, the XRD pattern displayed in Fig. 4 may be used to validate the existence of Si$_3$N$_4$ reinforcement on the magnesium surface. In accordance with the SEM findings, the XRD patterns clearly reveal the peaks that pertain to the Si$_3$N$_4$ reinforcement and the matrix.

3.2. Hardness properties

A material's hardness improved by adding hard ceramic materials. The increase in hardness on all produced surfaces can be attributed to silicon nitride's inherent hardness. The plastically deformed magnesium matrix material flows from the side to the groove, providing a continuous cast. When the reinforcement is stirred into the matrix as a whole, it results in a uniform dispersion of the Si$_3$N$_4$. This is responsible for considerable rise in hardness value in the stir region. The FSP reduces grain size, which means a decline in grain growth on the composite surface, thereby increasing the composite's hardness. The deterrent to dislocation
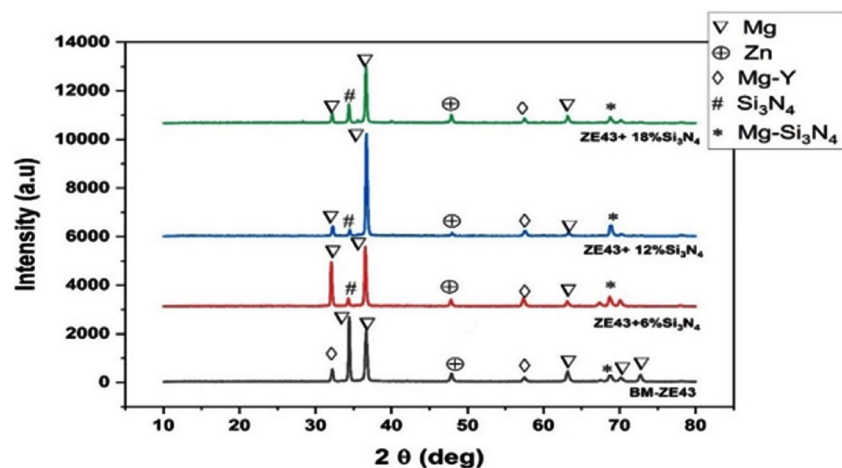
Fig. 4. XRD patterns of Magnesium ZE43 alloy and developed surface composites
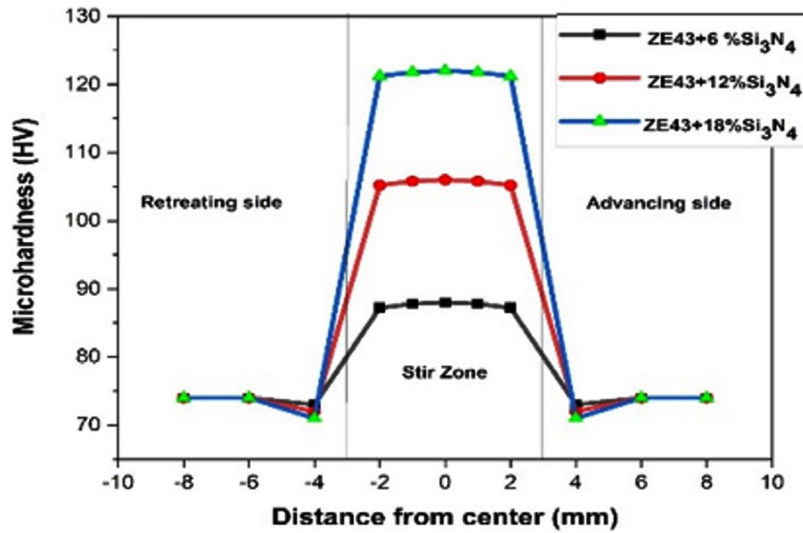
Fig. 5. Microhardness of Magnesium ZE43 alloy and developed surface composites

movement is caused by fine-grained silicon nitride particles. Also, the even distribution of reinforcements made of strong ceramic particles and the decrease in grain size caused by grain disintegration, annealing, and quenching during processing all make the surface composite much harder [23]. Analysis of the microstructure shows that the Si_3N_4 and the magnesium matrix form a strong bond, which makes the material harder. Fig. 5 shows that there is a correlation between the amount of reinforcement in a material and its subsequent increase in microhardness.

3.3. Potentiodynamic polarization (PDP)

The corrosion characteristics of base matrix material and the generated composites were investigated through potentiodynamic polarization. The typical characteristics of the potentiodynamic polarization measurement for ZE43 alloy and ZE43 + Si_3N_4 composites were determined after 72 hours of exposure are depicted in Fig. 6 and resulting polarization information is listed in

TABLE 3. All of the composites tested showed a higher corrosion potential (E_{corr}) compared to the alloy. This means that all of the composites' corrosion potentials were altered, for the better, by the addition of Si_3N_4 micro particles, and the composite made of 18% Si_3N_4 showed the best E_{corr} (–1485 mV).

When the Si_3N_4 micro particles were added, the corrosion potential of the developed composite showed considerable improvement, indicating its ability to resist corrosion. The ability of a material to resist corrosion can measure by its corrosion current density (I_{corr}). Corrosion current density values were reduced in this study by incorporating Si_3N_4 micro particles into the alloy. As evident in TABLE 3, compared to the base metal, all of the composites have much lower I_{corr} values. The composite containing 18% Si_3N_4 exhibited the lowest I_{corr} value of –0.770851 $\mu A/cm^2$, which was 47% less than that of the alloy (–0.405421 $\mu A/cm^2$). When comparing the corrosion current density of the processed composites and the base matrix material, a higher value indicated a quicker corrosion rate, whereas a lower value indicated a slower corrosion rate [31].
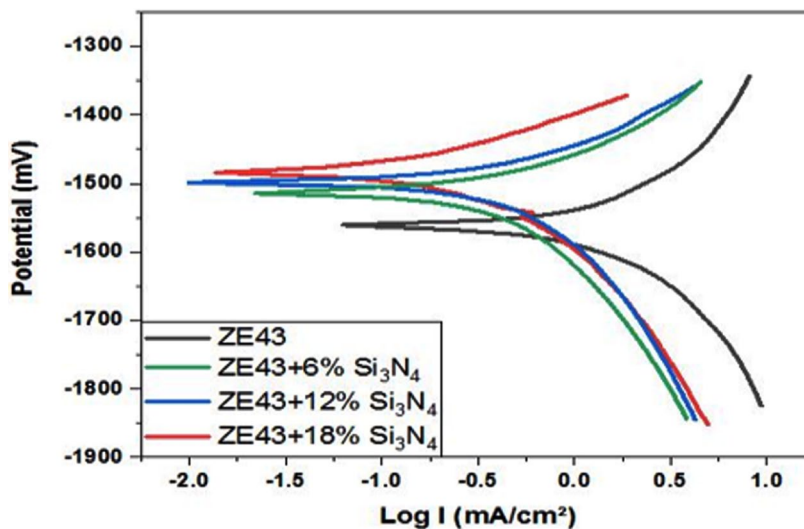
Fig. 6. Potentiodynamic polarization curves of Magnesium ZE43 alloy and developed surface composites

Electrochemical data of potentiodynamic polarization

Alloy/ Composite	E_{corr} (mV)	I_{corr} (µA/cm²)	R_{pol} (ohm/cm²)	β_a (mV)	β_c (mV)
ZE43	−1553	−0.405421	−2.46657	84.25362	−285.2156
ZE43 + 6% Si₃N₄	−1522	−0.422753	−2.36545	54.91301	−280.71781
ZE43 + 12% Si₃N₄	−1501	−0.453403	−2.20554	51.65958	−255.71497
ZE43 + 18% Si₃N₄	−1485	−0.770851	−1.29727	57.86176	−223.4799

3.4. Analysis of Wear Rate and COF using Experimental Design

The primary objective of the investigation was to use the Taguchi-GRA method to minimize the wear behavior performance characteristics of a friction stir processed composite, such as the wear rate, and friction coefficient. In the first step of analysis, the S/N ratios for the wear rate and friction coefficient were calculated.

As indicated previously, reduced values of wear rate and coefficient of friction result in superior wear performance; therefore, the MINITAB 19 software was used to calculate the signal to noise ratio. TABLE 4 displays the response characteristics and the corresponding values. TABLE 5 shows the raw data for the two response characteristics and their signal to noise ratio values.

The next step in the study is the normalizing of data for each performance indicator. TABLE 6 displays the normalized numbers and the associated deviation sequence. For determining grey relation coefficients (GRCs), the deviation sequences have been worked out. Then the GRC was calculated for each response characteristic utilizing the values of the deviation sequences listed in TABLE 6. The grey relation grades (GRGs) for each performance characteristic have been calculated. The values of the GRC and GRG along with the rank is displayed in TABLE 7. All grey relational grade values systematically vary from 0 and 1. A strong link can be observed between the reference sequence and the comparison sequence as the value of GRG approaches its maximum. Using the main effects evaluation of the Taguchi method, the average value of the GRG for each level of process factors has been determined, and the highest value has been selected for each factor to determine the optimal level of

Taguchi L_{27} OA and Trial results

	Input process factors			Experimental response data	
Exp. No.	Si₃N₄ Vol.(%) (A)	Load (N) (B)	Sliding Distance (m) (C)	Wear rate ×10⁻⁴ mm³/m	COF
1	6	5	500	0.51	0.399
2	6	5	1000	0.67	0.409
3	6	5	1500	1.23	0.438
4	6	10	500	0.1	0.43
5	6	10	1000	0.13	0.44
6	6	10	1500	0.24	0.452
7	6	15	500	0.15	0.446
8	6	15	1000	0.2	0.449
9	6	15	1500	0.37	0.458
10	12	5	500	0.38	0.378
11	12	5	1000	0.5	0.398
12	12	5	1500	0.93	0.423
13	12	10	500	0.76	0.415
14	12	10	1000	1.01	0.433
15	12	10	1500	1.85	0.448
16	12	15	500	1.14	0.436
17	12	15	1000	1.51	0.445
18	12	15	1500	0.28	0.456
19	18	5	500	0.2	0.348
20	18	5	1000	0.27	0.362
21	18	5	1500	0.49	0.396
22	18	10	500	0.4	0.382
23	18	10	1000	0.54	0.403
24	18	10	1500	0.99	0.426
25	18	15	500	0.61	0.408
26	18	15	1000	0.8	0.418
27	18	15	1500	1.48	0.443

TABLE 5

Experimental results and S/N ratios

Experimental response data			S/N ratios		Experimental response data			S/N ratios	
Exp. No.	Wear rate ×10⁻⁴ mm³/m	COF	S/N$_{Wear\ rate}$	S/N$_{COF}$	Exp. No.	Wear rate ×10⁻⁴ mm³/m	COF	S/N$_{Wear\ rate}$	S/N$_{COF}$
1	0.51	0.399	42.96709	3.990271	15	1.85	0.448	37.32828	3.48722
2	0.67	0.409	41.73925	3.882767	16	1.14	0.436	39.43095	3.605135
3	1.23	0.438	39.10095	3.585259	17	1.51	0.445	38.21023	3.5164
4	0.1	0.43	40	3.665315	18	0.28	0.456	35.55955	3.410352
5	0.13	0.44	38.86057	3.565473	19	0.2	0.348	46.94649	4.584208
6	0.24	0.452	36.17983	3.448616	20	0.27	0.362	45.71865	4.412914
7	0.15	0.446	38.18156	3.506651	21	0.49	0.396	43.06625	4.023048
8	0.2	0.449	36.9897	3.477537	22	0.4	0.382	43.93619	4.179366
9	0.37	0.458	34.31798	3.391345	23	0.54	0.403	42.70835	3.94695
10	0.38	0.378	44.21647	4.225082	24	0.99	0.426	40.05595	3.705904
11	0.5	0.398	42.98864	4.001169	25	0.61	0.408	42.17527	3.893398
12	0.93	0.423	40.33624	3.736596	26	0.8	0.418	40.94744	3.788237
13	0.76	0.415	41.20617	3.819519	27	1.48	0.443	38.29738	3.535963
14	1.01	0.433	39.95679	3.635121					

TABLE 6

Normalized S/N ratio and corresponding Deviation Sequence

Reference Sequence					Reference Sequence				
Normalized S/N ratio		Deviation Sequence			Normalized S/N ratio		Deviation Sequence		
Exp. No.	Wear rate	COF	Wear rate	COF	Exp. No.	Wear rate	COF	Wear rate	COF
1	0.684887	0.50209132	0.315113	0.49790868	15	0.238373	0.0803736	0.761627	0.9196264
2	0.58766	0.41196849	0.41234	0.58803151	16	0.404875	0.17922427	0.595125	0.82077573
3	0.378744	0.16256165	0.621256	0.83743835	17	0.308211	0.10483579	0.691789	0.89516421
4	0.449936	0.22967464	0.550064	0.77032536	18	0.098315	0.0159334	0.901685	0.9840666
5	0.359709	0.14597495	0.640291	0.85402505	19	1	1	0	0
6	0.147432	0.04801093	0.852568	0.95198907	20	0.902773	0.85640148	0.097227	0.14359852
7	0.305941	0.09666345	0.694059	0.90333655	21	0.69274	0.529569	0.30726	0.470431
8	0.211562	0.07225592	0.788438	0.92774408	22	0.761627	0.66061366	0.238373	0.33938634
9	0	0	1	1	23	0.664399	0.46577405	0.335601	0.53422595
10	0.783821	0.69893797	0.216179	0.30106203	24	0.454366	0.26370083	0.545634	0.73629917
11	0.686594	0.51122752	0.313406	0.48877248	25	0.622187	0.42088105	0.377813	0.57911895
12	0.476561	0.2894308	0.523439	0.7105692	26	0.52496	0.33272235	0.47504	0.66727765
13	0.545448	0.35894654	0.454552	0.64105346	27	0.315113	0.12123571	0.684887	0.87876429
14	0.446514	0.20436207	0.553486	0.79563793					

TABLE 7

GRC, GRG value and its rank

GRC			GRG	RANK	GRC			GRG	RANK
Exp. No.	Wear rate	COF			Exp. No.	Wear rate	COF		
1	0.613412214	0.50104785	0.55723	7	15	0.39631379	0.352205341	0.37426	23
2	0.548041435	0.459545515	0.503793	10	16	0.456568996	0.378565407	0.417567	17
3	0.445928374	0.373849009	0.409889	18	17	0.419537464	0.358380754	0.388959	21
4	0.476161412	0.39359995	0.434881	15	18	0.356713486	0.336912104	0.346813	26
5	0.438484481	0.369269386	0.403877	19	19	1	1	1	1
6	0.369667209	0.34435521	0.357011	25	20	0.837202301	0.776881837	0.807042	2
7	0.418739899	0.356293721	0.387517	22	21	0.619378902	0.515234985	0.567307	5
8	0.38806693	0.350202819	0.369135	24	22	0.67716411	0.595673259	0.636419	4
9	0.333333333	0.333333333	0.333333	27	23	0.59837195	0.483453348	0.540913	8
10	0.698149836	0.624171388	0.661161	3	24	0.478178903	0.404432853	0.441306	14
11	0.614699287	0.505677506	0.560188	6	25	0.569597411	0.463340949	0.516469	9
12	0.48854893	0.413028848	0.450789	13	26	0.512799372	0.428347104	0.470573	12
13	0.523805883	0.438191565	0.480999	11	27	0.421981011	0.362643568	0.392312	20
14	0.474614751	0.385910283	0.430263	16					

Fig. 7. Main effect plot for GRG

process factors for wear rate and COF. Using the information in the Fig. 7, we can figure out the optimum values for the process factors with the combination of A3B1C1, producing the largest values for the grey relation grade.

The significance and contribution of each process element to the GRG value have been determined by analysis of variance. TABLE 8 shows the response table for the GRG value. TABLE 9 shows the results of an ANOVA calculation for the combined response of wear rate and COF, including the F-ratio value and the percentage contribution of each process element. From the ANOVA calculation table, we can deduce that the factors Load (B) and Volume % of Si_3N_4 (A) contribute 37.13 and 27.57 percent towards the process, respectively, and that the factor sliding distance (C) contributes 19.36% towards the process.

3.5. Optimal Condition prediction using Desirability Function

On a scale from 0 to 1, desirability is a mathematical method for determining the optimal condition. To find the optimum condition, the total desirability value is used. Optimal performance was achieved by selecting the FSP condition with the highest total desirability value. The overall composite desirability is shown as a graph in Fig. 8. Overall, we have a composite desirability of 0.8578. Accordingly, the optimum parameters were 18% Si_3N_4

TABLE 8

Response table for GRG value

Level	Volume Percentage (%)	Load N	Sliding Distance (m)
1	0.4174	0.6130	0.5658
2	0.4568	0.4555	0.4972
3	0.5969	0.4025	0.4081
Delta	0.1795	0.2105	0.1577
Rank	2	1	3

The established mathematical model is represented by the following regression equation.

GRG = 0.4904-0.0730 Volume %_60.0336 Volume %_12 +
+ 0.1066 Volume %_18 + 0.1227 Load in N_5 − 0.0348
Load in N_10 − 0.0879 Load in N_15 + 0.0754 Sliding
Distance m_500 + 0.0068 Sliding Distance m_1000 − 0.0823
Sliding Distance m_1500

Fig. 8. Process parameter desirability graph

TABLE 9

ANOVA table for GRG value

Factor	DOF	Sum of Square	Mean Square	F Ratio	P Ratio	% Contribution
Volume %	2	0.16026	0.080129	17.29	0.000	27.57
Load N	2	0.21581	0.107907	23.28	0.000	37.13
Sliding Distance m	2	0.11253	0.056264	12.14	0.000	19.36
Residual Error	20	0.09270	0.004635			15.94
Total	26	0.58130				

volume, 5 N load, and 500 m sliding distance. A COF of 0.3577 and a wear rate of 0.00002 mm³/m are the optimal response parameters from the desirability graph.

3.6. Confirmation test

To validate the results of the investigation into the wear behavior and friction coefficient of ZE43 matrix composites reinforced with varying volume% of Si_3N_4 particles, tests have been run using the optimized settings (at 18% volume of Si_3N_4, 5 N load, and 500 m sliding distance). The developed composite was tested for wear behavior, and the findings showed a wear rate of 0.0000198 mm³/ m and a coefficient of friction of 0.3502 after the confirmatory test. TABLE 10 details the comparison of the response from multi response optimization with the Values obtained after optimal parameter setting, which revealed an increase in wear performance.

3.7. Worn-out surface characterizations

The worn out surfaces of both base matrix material and the developed composite surfaces shown in Fig. 9. The most prevalent sources of wear found by SEM analysis of worn surfaces were gross plastic changes, including delamination and micro fractures. Due to the malleability of magnesium, adhesive wear may also be seen with SEM.

When magnesium moves over a hard, rotating steel disc, it causes permanent deformation that helps material removal. The friction between the magnesium and rotating disc creates heat, which causes the metal to soften so that small pieces can go through the surface and make deep grooves. Therefore, most sample surfaces are characterized by the presence of grooves that point in the direction of sliding [32]. These grooves may have been formed by sharp protrusions on the counter face or by fragments that were released from the pin or disc as soon as it made contact with the surface. As seen in Fig. 9(b-d), the groove depth decreases, indicating surface is becoming more resistant to wear. Adding more reinforcements to a composite makes it harder, which makes it harder to break through the surface. In this way, material loss from the sliding surface is decreased as the percentage of reinforcing particles increases.

4. Conclusion

The friction stir processing was used to make a high-performance ZE43 magnesium surface composite with Si_3N_4 reinforcement. Following are the conclusions that can be made after examining the microstructure, microhardness, and tribological behavior of the composite that was developed:

1. The microstructure of the composites that were made showed that the grains got smaller during FSP and that the reinforcement was spread out evenly in the magnesium matrix material.
2. The 18% silicon nitride surface composite created has the highest hardness (122 ± 2.3 VHN) out of all the surface composites. The reason for this is that the processed composite's surface features a uniform dispersion of hard Si_3N_4 particles.
3. The corrosion potential (E_{corr}) of all the developed composites is greater than that of the base material. Among the developed composites, the one that has the highest corrosion resistance ($E_{corr} = -1485$ mV) is the one that contains 18% Si_3N_4.
4. Variations in the volume percentage of Si_3N_4, the load, and the sliding distance were used to obtain wear rate values for the L_{27} orthogonal array. The multi-objective problem was

TABLE 10

Confirmation test results

Optimal parameter setting			Process parameters	Response from Multi response optimization	Response from confirmation test
Volume (%)	Load (N)	Sliding Distance (m)			
18	5	500	Wear rate mm³/m	0.0000202	0.0000198
			COF	0.3577	0.3502
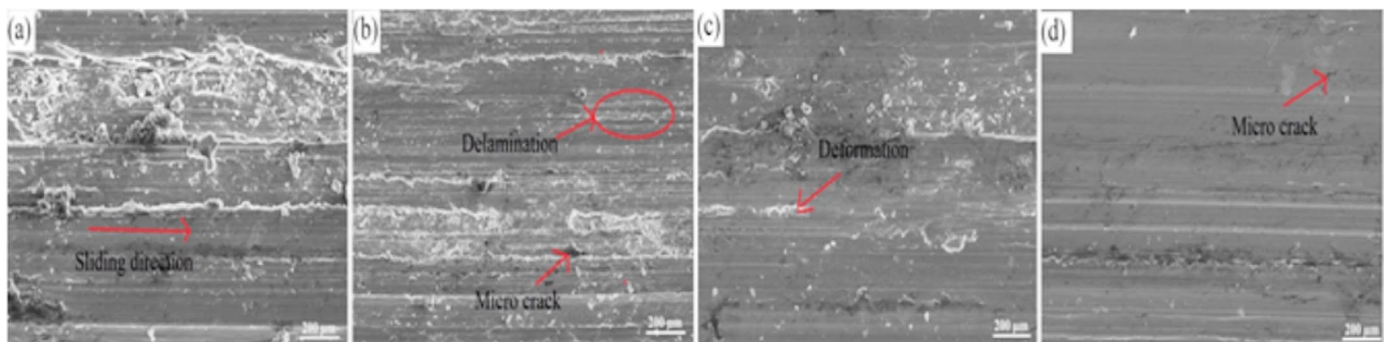
Fig. 9. SEM images showing a worn out surface of Magnesium ZE43 base matrix material and developed surface composites

reduced to a single-objective one by using Grey Relational Analysis. On the 19th trial, GRG reached its maximum value of 1 (A3B1C1).

5. The maximum wear resistance was achieved when the volume percentage of Si_3N_4 was high (18%), the load was low (5 N), and the sliding distance was short (500 m). Confirmation trials were done based on the optimal parameter setting, and the response values revealed an increase in wear performance.

Availability of data and material

This work is a part of the ongoing research. The article contains all of the data necessary for this investigation.

REFERENCES

[1] V. Sharma, U. Prakash, B. V. M. Kumar, Surface composites by friction stir processing: A review. Journal of Materials Processing Technology, **224**, 117-134 (2015).
DOI: https://doi.org/10.1016/j.jmatprotec.2015.04.019

[2] K. K. Chawla, Metal Matrix Composites. In K.K. Chawla (Ed.), Composite Materials: Science and Engineering (p. 197-248). New York, NY: Springer New York. (2012).
DOI: https://doi.org/10.1007/978-0-387-74365-3_6

[3] L. Singh, B. Singh, K. K. Saxena, Manufacturing techniques for metal matrix composites (MMC): an overview. Advances in Materials and Processing Technologies **6** (2), 441-457 (2020).
DOI: https://doi.org/10.1080/2374068X.2020.1729603

[4] S. Dadbakhsh, R. Mertens, L. Hao, J.V. Hambeeck, J.P Kruth, Selective Laser Melting to Manufacture "In Situ" Metal Matrix Composites: A Review. Adv. Eng. Mater. **21**, 1801244 (2019).
DOI: https://doi.org/10.1002/adem.201801244

[5] J. Xu, B. Zou, S. Tao, M. Zhang, X. Cao, Fabrication and properties of Al_2O_3–TiB_2–TiC/Al metal matrix composite coatings by atmospheric plasma spraying of SHS powders. J. Alloys Compd. **672**, 251-259 (2016).
DOI: https://doi.org/10.1016/j.jallcom.2016.02.11

[6] X. Yang, W. Wang, W. Ma, Y. Wang, J. Yang, S. Liu, H. Tang, Corrosion and wear properties of micro-arc oxidation treated Ti6Al4V alloy prepared by selective electron beam melting. Trans. Nonferrous Met. Soc. China **30**, 2132-2142 (2020).
DOI: https://doi.org/10.1016/S1003-6326(20)65366-3

[7] R. Butola, D. Pandit, C. Pratap, P. Chandra, Two decades of friction stir processing – a review of advancements in composite fabrication. J. Adhes. Sci. Technol. **36**, 795-832 (2022).
DOI: https://doi.org/10.1080/01694243.2021.1938835

[8] R.S. Mishra, Z.Y. Ma, I. Charit, Friction stir processing: a novel technique for fabrication of surface composite. Mater. Sci. Eng. A **341**, 307-310 (2003).
DOI: https://doi.org/10.1016/S0921-5093(02)00199-5

[9] R. Taghiabadi, A. Moharami, Mechanical properties enhancement of Mg–4Si in-situ composites by friction stir processing. Mater. Sci. Technol. **37**, 66-77 (2021).
DOI: https://doi.org/10.1080/02670836.2020.1866848

[10] J. Iwaszko, K. Kudła, Microstructure, hardness, and wear resistance of AZ91 magnesium alloy produced by friction stir processing with air-cooling. Int. J .Adv. Manuf. Technol. **116**, 1309-1323 (2021). DOI: https://doi.org/10.1007/s00170-021-07474-9

[11] M. Balakrishnan, I. Dinaharan, K. Kalaiselvan, R. Palanivel, Friction stir processing of Al_3Ni intermetallic particulate reinforced cast aluminum matrix composites: Microstructure and tensile properties. J. Mater. Res. Technol. **9**, 4356-4367 (2020).
DOI: https://doi.org/10.1016/j.jmrt.2020.02.060

[12] H. Yamamoto, Y. Imagawa, K. Ito, K. Chen, L. Zhang, Alloying a topmost steel-plate layer with WC-tool constituent elements during friction stir processing. J. Manuf. Process. **69**, 311-319 (2021). DOI: https://doi.org/10.1016/j.jmapro.2021.07.050

[13] M. Vakili-Azghandi, M. Roknian, J.A. Szpunar, S.M. Mousavizade, Surface modification of pure titanium via friction stir processing: Microstructure evolution and dry sliding wear performance. Journal of Alloys and Compounds **816**, 152557 (2020).
DOI: https://doi.org/10.1016/j.jallcom.2019.152557

[14] H. Tripathi, A. Bharti, K.K. Saxena, N. Kumar, Improvement in mechanical properties of structural AZ91 magnesium alloy processed by friction stir processing. Advances in Materials and Processing Technologies **8**, 1543-1556 (2022).
DOI: https://doi.org/10.1080/2374068X.2021.1949540

[15] A.Z. Naser, B.M. Darras, Experimental investigation of Mg/SiC composite fabrication via friction stir processing. Int. J. Adv. Manuf. Technol. **91**, 781-790 (2017).
DOI: https://doi.org/10.1007/s00170-016-9801-z

[16] F. Long, G. Chen, M. Zhou, Q. Shi, Q. Liu, Simultaneous enhancement of mechanical properties and corrosion resistance of as-cast Mg-5Zn via microstructural modification by friction stir processing. Journal of Magnesium and Alloys **11** (6), 1931-1943 (2021). DOI: https://doi.org/10.1016/j.jma.2021.08.029

[17] S. Sudhagar, P.M. Gopal, Investigation on Mechanical and Tribological Characteristics Cu/Si_3N_4 Surface Composite Developed Through Friction Stir Processing. Silicon **14**, 4207-4216 (2022).
DOI: https://doi.org/10.1007/s12633-021-01206-0

[18] P. Maji, R.K. Nath, P. Paul, R.K. Bhogendro Meitei, S.K. Ghosh, Effect of processing speed on wear and corrosion behavior of novel MoS_2 and CeO_2 reinforced hybrid aluminum matrix composites fabricated by friction stir processing. Journal of Manufacturing Processes **69**, 1-11 (2021).
DOI: https://doi.org/10.1016/j.jmapro.2021.07.032

[19] M. Azizieh, A.H. Kokabi, P. Abachi, Effect of rotational speed and probe profile on microstructure and hardness of AZ31/Al2O3 nanocomposites fabricated by friction stir processing. Mater. Des. **32**, 2034-2041 (2011).
DOI: https://doi.org/10.1016/j.matdes.2010.11.055

[20] Y. Mazaheri, M.M. Jalilvand, A. Heidarpour, A.R. Jahani, Tribological behavior of AZ31/ZrO_2 surface nanocomposites developed by friction stir processing. Tribol. Int. **143**, 106062 (2020).
DOI: https://doi.org/10.1016/j.triboint.2019.106062

[21] S. Abazari, A. Shamsipur, H.R. Bakhsheshi-Rad, A.F. Ismail, S. Sharif, M. Razzaghi, S. Ramakrishna, F. Berto, Carbon Nanotubes (CNTs)-Reinforced Magnesium-Based Matrix Composites: A Comprehensive Review. Materials (Basel) **13**, 4421 (2020). DOI: https://doi.org/10.3390/ma13194421

[22] R.K. Saranu, R. Chanamala, S.R. Putti, G.K. Mallarapu, Investigation of Microstructures, Mechanical Properties of AZ91E Hybrid Composite Reinforced with Silicon Carbide and Fly Ash. Silicon **13**, 2145-2156 (2021). DOI: https://doi.org/10.1007/s12633-020-00671-3

[23] S. Joshi, N. Yuvaraj, R.C. Singh, R. Chaudhary, Microstructural and Wear Investigations of the Mg/B$_4$C Surface Composite Prepared Through Friction Stir Processing. Trans. Indian. Inst. Met. **73**, 3007-3018 (2020). DOI: https://doi.org/10.1007/s12666-020-02102-8

[24] P. Krishnan, P. Lakshmanan, G. Annamalai, Impact of nano-SiC$_P$ and nano-hBN$_P$ on the corrosion performance and fatigue behavior of Mg–Zn hybrid nanocomposites. Mater. Corros. **74**, 403-418 (2023). DOI: https://doi.org/10.1002/maco.202213523

[25] T. Thankachan, K. Soorya Prakash, V. Kavimani, S.R. Silambarasan, Machine Learning and Statistical Approach to Predict and Analyze Wear Rates in Copper Surface Composites. Met. Mater. Int. **27**, 220-234 (2021). DOI: https://doi.org/10.1007/s12540-020-00809-3

[26] A. Abbas, V. Rajagopal, S.J. Huang, Magnesium Metal Matrix Composites and Their Applications. In: Tański T. Jarka P. (eds) Magnesium Alloys Structure and Properties. IntechOpen, Rijeka, p Ch. **8** (2021). DOI: https://doi.org/10.5772/intechopen.96241

[27] U. Çaydaş, A. Hasçalık, Use of the grey relational analysis to determine optimum laser cutting parameters with multi-performance characteristics. Opt. Laser Technol. **40**, 987-994 (2008). DOI: https://doi.org/10.1016/j.optlastec.2008.01.004

[28] D. Ju-Long, Control problems of grey systems. Syst. Control. Lett. **1**, 288-294 (1982). DOI: https://doi.org/10.1016/S0167-6911(82)80025-X

[29] R. Sathiskumar, N. Murugan, I. Dinaharan, S.J. Vijay, Characterization of boron carbide particulate reinforced in situ copper surface composites synthesized using friction stir processing. Mater. Charact. **84**, 16-27 (2013). DOI: https://doi.org/10.1016/j.matchar.2013.07.001

[30] T. Thankachan, K. Soorya Prakash, Microstructural, mechanical and tribological behavior of aluminum nitride reinforced copper surface composites fabricated through friction stir processing route. Materials Science & Engineering A **688**, 301-308 (2017). DOI: https://doi.org/10.1016/j.msea.2017.02.010

[31] S. Kandasamy, P. Rathinasamy, N. Nagarajan, K. Arumugan, R. Rathanasamy, G.V. Kaliyannan, Corrosion behavioral studies on AA7075 surface hybrid composites tailored through friction stir processing. Anti-Corrosion Methods Mater. **67**, 345-355 (2020). DOI: https://doi.org/10.1108/ACMM-11-2019-2215

[32] N. Radhika, P. Rajpurohit, A. Diwakar, Synthesis of Al LM25/ TiB2 in-situ composites and investigation of its adhesive wear behavior. Part. Sci. Technol. **38**, 184-192 (2020). DOI: https://doi.org/10.1080/02726351.2018.1526833